Intramolecular Charge-Transfer Dynamics in Covalently Linked Perylene−Dimethylaniline and Cyanoperylene−Dimethylaniline

Natalie Banerji, Gonzalo Angulo,† Igor Barabanov,‡ and Eric Vauthey*

Department of Physical Chemistry, University of Geneva, 30 quai Ernest-Ansermet, CH-1211 Geneva 4, Switzerland

Received: April 25, 2008; Revised Manuscript Received: July 3, 2008

The excited-state dynamics of covalently linked electron donor−acceptor systems consisting of *N*,*N*-dimethylaniline (DMA) as electron donor and either perylene (Pe) or cyanoperylene (CNPe) as acceptor has been investigated in a large variety of solvents, including a room-temperature ionic liquid, by using femtosecond time-resolved fluorescence and absorption spectroscopy. The negligibly small solvent dependence of the absorption spectrum of both compounds and the strong solvatochromism of the fluorescence are interpreted by a model where optical excitation results in the population of a locally excited state (LES) and emission takes place from a charge-separated state (CSS). This interpretation is supported by the fluorescence up-conversion and the transient absorption measurements that reveal substantial spectral dynamics in polar solvents only, occurring on time scales going from a few hundreds of femtoseconds in acetonitrile to several tens of picoseconds in the ionic liquid. The early transient absorption spectra are similar to those found in nonpolar solvents and are ascribed to the LES absorption. The late spectra due to CSS absorption show bands that are red-shifted relative to those of the radical anion of the acceptor moiety by an amount that depends on solvent polarity, pointing to partial charge separation. Global analysis of the time-resolved data indicates that the charge separation dynamics in PeDMA is essentially solvent controlled, whereas that in CNPeDMA is faster than diffusive solvation, this difference being accounted for by a larger driving force for charge separation in the latter. On the other hand, the CSS lifetime of PeDMA is of the order of a few nanoseconds independently of the solvent, whereas that of CNPeDMA decreases with increasing solvent polarity from a few nanoseconds to a few hundreds of picoseconds. Comparison of these results with previously published data on the fluorescence quenching of Pe and CNPe in pure DMA shows that the charge separation and the ensuing charge recombination occur on similar time scales independently of whether these processes are intra- or intermolecular.

Introduction

In 1961, Leonhardt and Weller reported the first direct evidence of fluorescence quenching by electron transfer by using perylene (Pe) and *N*,*N*-dimethylaniline (DMA) as acceptor (A) and donor (D), respectively.[1] Since then, photoinduced electron transfer has probably been the most investigated reaction in photochemistry. Indeed, tremendous effort has and is still being invested to understand the fine details of both intra- and intermolecular charge transfer (CT) processes.[2,3] Although an impressively large number of molecular systems, going from directly linked DA compounds to highly sophisticated architectures of D and A units, have been elaborated,[4−9] and although DMA and Pe represent a prototypic pair for intermolecular electron transfer studies,[1,10−16] intramolecular CT in covalently linked PeDMA has never been investigated so far.

We report here on a detailed study of the excited-state dynamics of two covalently linked DA systems consisting in DMA as electron donor and Pe or cyanoperylene (CNPe) as acceptor (Chart 1) by using femtosecond-resolved fluorescence and absorption spectroscopy. The measurements have been performed in a series of solvents, including a room-temperature ionic liquid, differing by their polarity and dynamic properties. There are two main reasons for studying intramolecular CT in these molecules:

CHART 1

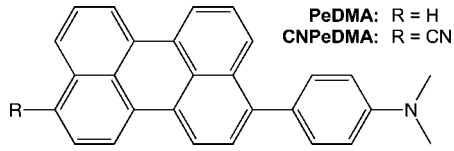

1. Intramolecular CT in DA systems consisting of DMA covalently linked to anthracene (ADMA),[17−20] pyrene (PyDMA),[19,21] and phenanthrene (PhDMA)[22] has already been reported. Although these compounds are structurally relatively similar, somewhat different models have been proposed to account for their excited-state dynamics. For ADMA, which has been the most studied,[17−20] the observed dynamics is best explained as a transition from a locally excited state (LES) to a charge-separated state (CSS) involving both the solvation and the twist angle between the DMA and anthracene aromatic planes as relevant coordinates.[20] The intramolecular charge separation (CS) dynamics was thus found to be solvent dependent and somewhat slower than the corresponding solvation dynamics, especially in moderately polar solvents. Intramolecular CS has

* Corresponding author. E-mail: eric.vauthey@chiphy.unige.ch.
† Present address: Institute of Physical Chemistry, Polish Academy of Sciences, Warsaw, Poland.
‡ Permanent address: Institute of Chemical Kinetics and Combustion, Siberian Branch of the Russian Academy of Sciences, Novosibirsk, Russian Federation.

10.1021/jp803621z CCC: $40.75
Published on Web 09/06/2008

also been observed in ADMA para-substituted with a cyano-group in (CNADMA),[23] but its detailed dynamics has not been reported.

The time-resolved fluorescence and transient absorption (TA) results obtained with PyDMA in hexanol and octanol were discussed by using a scheme where direct optical population of a CSS is followed by solvent relaxation occurring in parallel to radiative and nonradiative charge recombination (CR) to the ground state.[21] Finally, according to ref 22, excitation of PhDMA in acetonitrile results in a LES and is followed by a subpicosecond population of a hot CSS relaxing on the picosecond time scale. The ensuing equilibrated CSS population decays both to the ground state by fluorescence and to a triplet state by intersystem crossing.

In all these investigations, the LES and CSS were identified by their distinct emission and TA spectra. The emission spectrum of the LES resembles the mirror image of the S_0-LES absorption band, whereas that of the CSS is broad, red-shifted, and similar to the steady-state fluorescence spectrum.[18] On the other hand, the absorption spectrum of the LES is close to the S_1-state spectrum of the chromophoric acceptor unit, whereas that of the CSS was found to be very similar to the composite spectrum of the donor cation and acceptor anion.[17,20] However, it should be noted that DMA radical cation exhibits only a small absorption band peaking at 475 nm, whereas the radical anion bands of the acceptor units and especially those of anthracene are relatively broad and weak throughout the visible region.[24] Therefore, the extent of charge separation of the CSS is difficult to determine from the TA spectra. Pe differs substantially from anthracene in this respect, because its S_1 state, T_1 state, and radical anion exhibit intense and distinct absorption bands in the 450−700 nm region.[1,11,24] Therefore, rather precise information on the nature of the excited state can be expected from TA measurements on PeDMA and CNPeDMA.

2. The fluorescence quenching of Pe and CNPe in DMA as electron-donating solvent has been recently reported.[25,26] This approach was used to determine the intrinsic bimolecular CS dynamics without the complications arising from the translational diffusion of the reactants. Although the driving force of photoinduced CS with Pe is only about 0.1 eV smaller than that with CNPe, the average quenching time constant was found to be about 10 times larger with Pe ($\tau_q = 4.9$ ps) than with CNPe ($\tau_q = 470$ fs). This surprising difference was explained with a model where the number of donor molecules with an optimal orientation for CS is larger with CNPe than with Pe because dipole−dipole interaction between the polar CNPe and DMA favors mutual orientations with a large electronic coupling. The experimental data could be reproduced with this model by assuming the same intrinsic time constant for CS with both Pe and CNPe ($\tau_{CS} \approx 1$ ps).[25,26]

Consequently, PeDMA and CNPeDMA offer a unique opportunity to investigate the CS dynamics in conditions where Pe and CNPe interact with a single DMA unit only and where diffusion of the reactants is eliminated. Thus, if the above-mentioned model used to account for the quenching in pure DMA is correct, the intramolecular CS dynamics in these two covalently linked DA systems should not differ very strongly.

Comparison of PeDMA and CNPeDMA with Pe and CNPe in DMA should additionally give a new insight into the effect of direct covalent bonding and mutual orientation of the donor and acceptor moieties on both CS and CR dynamics.

Experimental Section

The synthesis of 3-(*p*-*N*,*N*-dimethylaminophenyl)perylene (PeDMA) has already been reported in ref 27. The synthesis of 3-cyano-10-(*p*-*N*,*N*-dimethylaminophenyl)perylene (CNPeDMA) is described in detail in the Supporting Information. The final product consists in a mixture, most probably 1:1, of 3-cyano-9-(*p*-*N*,*N*-dimethylaminophenyl)perylene and 3-cyano-10-(*p*-*N*,*N*-methylaminophenyl)perylene. As shown later on, both isomers have essentially the same photophysical properties. The solvents hexane (HX), octane (OCT), cyclohexane (CHX), *p*-xylene (PXY), toluene (TOL), diethylether (DIE), chloroform ($CHCl_3$), tetrahydrofuran (THF), 1-pentanol (PnOH), 2-propanol (PrOH), acetone (ACE), benzonitrile (BCN), methanol (MeOH), acetonitrile (ACN), dimethylsulfoxide (DMSO), and the ionic liquid (IL), 1-ethyl-3-methyl-imidazolium-ethylsulfate (Ecoeng212, Solvent Innovation GmbH), were of the highest commercially available purity and were used as received. The solutions were deoxygenated by Ar bubbling before all measurements.

Steady-State Measurements. Absorption spectra were recorded on a Cary 50 spectrophotometer, and fluorescence spectra were measured on a Cary Eclipse fluorimeter. Fluorescence spectra were corrected for the wavelength-dependent sensitivity of the detection. Quantum yield measurements were performed against Pe in ACN ($\Phi_{fl} = 0.87$).[28] For fluorescence measurements, the absorbance of the sample solutions was adjusted to a value of 0.1 on 1 cm at the band maximum.

Time-Resolved Fluorescence. Fluorescence lifetime measurements on the nanosecond time scale were carried out with the time-correlated single photon counting (TCSPC) technique as described elsewhere.[29] Excitation was performed at a repetition rate of 10 MHz with ~60 ps pulses generated with laser diodes at 395 nm and at 469 nm (Picoquant models LDH−P-C-400B and LDH−P-C-470). The full width at half maximum (fwhm) of the instrument response function was around 200 ps. The solute concentrations were the same as those for the steady-state measurements.

Experiments on shorter time scales were performed by using fluorescence up-conversion as discussed in detail before.[30] Excitation was achieved at 400 nm with the frequency-doubled output of a Kerr lens mode-locked Ti:Sapphire laser (Tsunami, Spectra-Physics). The polarization of the pump beam was at magic angle relative to that of the gate pulses at 800 nm. Time-resolved fluorescence anisotropy measurements were carried out by changing the polarization of the pump beam with respect to the gate beam with a half-wave plate. The anisotropy decay, $r(t)$, was reconstructed by using the standard equation, $r(t) = (I_{||}(t) - I_{\perp}(t))/(I_{||}(t) + 2I_{\perp}(t))$, where $I_{||}(t)$ and $I_{\perp}(t)$ are the fluorescence intensities recorded with the polarization of the pump beam set parallel and perpendicular to that of the gate beam, respectively. The 400 nm pump intensity on the sample was on the order of 5 $\mu J \cdot cm^{-2}$, and the fwhm of the instrument response function was ca. 210 fs. The sample solutions were located in a 0.4 mm thick rotating cell and had an absorbance of about 0.1.

Transient Absorption. The experimental setup has been described in detail earlier.[31] Excitation was performed either at 400 nm by using the frequency-doubled output of a standard 1 kHz amplified Ti:Sapphire system (Spectra-Physics) or at 490 nm with a home-built two-stages noncollinear optical parametric amplifier. The pump intensity on the sample was around 2 $mJ \cdot cm^{-2}$. The polarization of the probe pulses was at magic angle relative to that of the pump pulses. All spectra were corrected for the chirp of the white light probe pulses. The fwhm of the instrument response function was ca. 200 fs. The sample solutions were placed in a 1 mm thick quartz cell where they were continuously stirred by N_2 bubbling. Their absorbance at

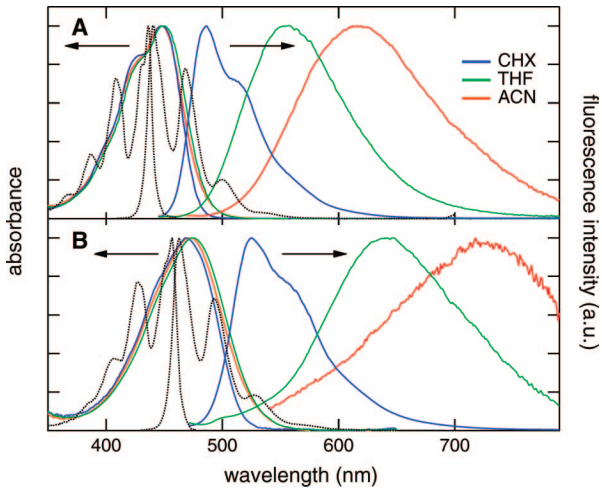

Figure 1. Absorption and fluorescence spectra of PeDMA (A) and CNPeDMA (B) in various solvents (solid lines) and of Pe (A) and CNPe (B) in CHX (dotted lines).

the excitation wavelength was between 0.05 and 0.2, depending on the solvent.

Quantum Chemistry Calculations. Ground-state electric dipole moment calculation of PeDMA in the gas phase was performed at the density functional level of theory (DFT) by using the B3LYP functional[32] and a [3s2p1d] basis set. The calculations were carried out by using Turbomole version 5.9.[33]

Results and Discussion

Steady-State Spectroscopy. Absorption and fluorescence spectra of PeDMA and CNPeDMA recorded in solvents of varying polarity are shown in Figure 1. These spectra differ substantially from those of the parent Pe and CNPe chromophores, which both exhibit clear vibrational progressions in absorption and emission. A second absorption band of somewhat larger intensity can be observed around 260 nm (Figure S1, see Supporting Information). This band is substantially broader than the composite spectrum of the donor and acceptor units, which both absorb in this region as well.

The first absorption band maxima of PeDMA and CNPeDMA are also red-shifted relative to those of the parent chromophores (~660 and 560 cm^{-1} for Pe and CNPe in CHX, respectively) but present a very small solvent dependence (see Table 1). The solvatochromism of this absorption band seems to be dominated by dispersion interaction.[35] Indeed, the plot of the absorption maximum of PeDMA in wavenumber as a function of $f(n^2) = 2(n^2 - 1)/(2n^2 + 1)$, where n is the refractive index, exhibits a distinct linear correlation with a -4120 cm^{-1} slope (Figure S2, see Supporting Information). On the other hand, if solvents of similar refractive index are considered, a small red shift of the absorption maximum with the polarity function, $f(\varepsilon_s) = 2(\varepsilon_s - 1)/(2\varepsilon_s + 1)$, where ε_s is the static dielectric constant, can be observed, the slope being of the order of -400 cm^{-1}. According to the Onsager model,[35,36] this slope, expressed in Joule, corresponds to $-\vec{\mu}_g\Delta\vec{\mu}/(4\pi\varepsilon_0 a^3)$, where $\vec{\mu}_g$ is the permanent electric dipole moment of the molecule in the electronic ground state, $\Delta\vec{\mu}$ is the dipole moment difference vector between excited and ground states, ε_0 is the vacuum permittivity, and a is the cavity radius. This equation, with a cavity radius of $4.34 \cdot 10^{-10}$ m estimated from the Van der Waals increment method,[37] results in a value for $|\vec{\mu}_g\Delta\vec{\mu}|$ of $7.24 \cdot 10^{-59}$ C^2 m^2 (6.5 D^2). Assuming $\vec{\mu}_g$ and $\Delta\vec{\mu}$ to be parallel and taking $|\vec{\mu}_g| = 3.5$ D from DFT calculations yields $|\Delta\vec{\mu}| = 1.85$ D. This value should only be considered as a crude estimate but clearly points to a moderate increase of the electric dipole moment in the Franck−Condon excited state of PeDMA. CNPeDMA was not investigated in a sufficiently large number of solvents to allow such analysis to be performed. Despite this, the very small solvatochromism of its first absorption band (Table 2) indicates that similar conclusions can be drawn for this molecule.

TABLE 1: Photophysical Properties of PeDMA

solvent	ε_s[a]	λ_{abs}[b] (nm)	λ_{fl}[b] (nm)	Φ_{fl}[c]	τ_{fl}[d] (ns)	$\tau_{rad}n^3$[e] (ns)	τ_{nr}[f] (ns)
HX	1.88	446	487				
OCT	1.94	448	487				
CHX	2.02	449	487	1.0	3.4	9.9	≥170
PXY	2.27	453	508				
TOL	2.38	453	512				
DIE	4.33	446	518				
$CHCl_3$	4.81	452	536				
THF	7.58	450	556	0.77	4.6	16.5	20.0
PnOH	13.9	449	548	0.87	4.6	14.7	35.4
PrOH	19.92	447	558				
ACE	20.70	448	595	0.62	5.3	21.4	13.9
BCN	25.20	459	585	0.72	5.0	24.8	17.9
MeOH	32.70	445	582				
ACN	37.5	448	617	0.50	5.3	25.8	10.6
DMSO	46.68	455	641	0.32	4.1	36.5	6.0
IL		456	638				

[a] Static dielectric constant at 20 or 25 °C (from ref 34). [b] Absorption and fluorescence maxima. [c] Fluorescence quantum yield. [d] Fluorescence lifetime. [e] Solvent corrected radiative time constant. [f] Nonradiative time constant.

TABLE 2: Photophysical Properties of CNPeDMA

solvent	λ_{abs}[a] (nm)	λ_{fl}[a] (nm)	Φ_{fl}[b]	τ_{fl}[c] (ns)	$\tau_{rad}n^3$[d] (ns)	τ_{nr}[e] (ns)
CHX	469	524	1.0	3.6	10.4	≥180
THF	476	622	0.59	4.5	21.1	11.0
ACN	472	730	0.025	0.35[f]	34.0	0.36
DMSO	482	745	0.013	0.13[f]	32.3	0.13

[a] Absorption and fluorescence maxima. [b] Fluorescence quantum yield. [c] Fluorescence lifetime. [d] Solvent corrected radiative time constant. [e] Nonradiative time constant. [f] Determined from TA measurements.

The fluorescence spectrum of both DA compounds exhibits a much stronger solvent dependence. Except in nonpolar solvents, where some vibronic structure can be guessed, the broad and structureless band shape suggests a CT emission (Figure 1). The fluorescence quantum yield, Φ_{fl}, of PeDMA is unity in CHX and decreases with increasing solvent polarity (Table 1). For CNPeDMA, Φ_{fl} exhibits an even stronger solvent dependence. However, the measurement of the fluorescence spectrum of this compound in the most polar solvents was complicated by its small Φ_{fl} and by the presence of a highly fluorescing impurity that could not be totally eliminated even after repeated recristallisation. Contribution of this impurity to the fluorescence spectrum of CNPeDMA could only be avoided upon red-edge excitation.

A plot of the emission maximum of PeDMA versus $f(\varepsilon_s)$ - $f(n^2)$ shows a reasonably linear dependence with a -6700 cm^{-1} slope (Figure S3, see Supporting Information). The slope in Joule corresponds here to $-\vec{\mu}_e\Delta\vec{\mu}/(4\pi\varepsilon_0 a^3)$, where $\vec{\mu}_e$ is the permanent electric dipole moment of the molecule in the emitting state. This equation yields a value for $|\vec{\mu}_e\Delta\vec{\mu}|$ of $3.64 \cdot 10^{-28}$ C^2 m^2 (109 D^2). Taking $|\vec{\mu}_g| = 3.5$ D results in $|\vec{\mu}_e| = 12.3$ D and $|\Delta\vec{\mu}| = 8.8$ D. These two values are in complete contradiction with those obtained from the absorption solvatochromism. This inconsistency can be accounted for by an emitting state differing substantially from the Franck−Condon

excited state. Excitation in the first absorption band of PeDMA leads to the population of a moderately polar excited state that can be considered as a LES ($|\vec{\mu}_{LES}| \approx 5$ D), whereas emission arises essentially totally from a highly polar state, a CSS ($|\vec{\mu}_{CSS}| \approx 12$ D).

The first absorption band of ADMA and of DA compounds with acridine as acceptor has been shown to stem from the superposition of S_0-LES and S_0-CSS bands.[18,19] The presence of a S_0-CSS transition could be responsible for the broadening of the red side of the first absorption band of PeDMA and CNPeDMA observed by going from nonpolar to polar solvents (Figure 1). If this is the case, the oscillator strength of this transition is too small compared with that of the S_0-LES transition to affect significantly the solvatochromism of PeDMA and CNPeDMA absorption.

Another possibility to reconcile the absorption and emission solvatochromism without having to invoke a LES-CSS transition is to suppose that the calculated $|\vec{\mu}_g|$ value is incorrect. In this case, the $|\vec{\mu}_g \Delta\vec{\mu}|$ and $|\vec{\mu}_e \Delta\vec{\mu}|$ values obtained from the slope of the absorption and fluorescence solvatochromic plots, respectively, can be reproduced by assuming $|\vec{\mu}_g| = 0.65$ D, $|\vec{\mu}_e| = 10.8$ D and $|\Delta\vec{\mu}| = 10.15$ D. This hypothesis is nevertheless quite improbable as a ground-state dipole moment of $|\vec{\mu}_g| = 0.65$ D would be much smaller than those reported for ADMA and other DA compounds with DMA and aryl acceptors.[18,38−40]

The magnitude of the excited-state dipole moments depends strongly on the cavity radius and on the polarity function used for the calculation.[35,41,42] Despite this, the dipole moment of the CSS estimated here for PeDMA is substantially smaller than all those reported for other DA compounds with DMA and aryl acceptors.[17,38,40,42] For example, with pyrene and acridine as acceptors, $|\vec{\mu}_e|$ of 21 and 26 D have been found, respectively.[38,40] A $|\vec{\mu}_e| = 12.3$ D corresponds to a full charge separation over 2.5 Å or to the transfer of 0.4 electron over 6.6 Å, the center-to-center distance between the DA units. This again should be considered as a very crude estimate.

Time-Resolved Fluorescence. The fluorescence decay of PeDMA measured by TCSPC can be well reproduced using a single-exponential function (Figure S4, see Supporting Information) with the time constants listed in Table 1. Except for DMSO, the fluorescence lifetime of PeDMA increases weakly with the dielectric constant of the solvent. Table 1 shows that the radiative time constant calculated from the fluorescence lifetime and quantum yield and corrected for the solvent, $\tau_{rad}n^3$,[43] becomes larger with solvent polarity. This effect cannot be fully accounted for by the transition energy dependence of τ_{rad}. Indeed, the magnitude of the transition dipole moment for fluorescence, calculated from the radiative time constant (eq.(S1), see Supporting Information),[44] decreases from 6.2 D in CHX to 5.85 D in THF and to 4.9 D in DMSO, pointing to a solvent dependence of the nature of the emitting state. On the other hand, a parallel decrease of the time constant of nonradiative deactivation, τ_{nr}, with increasing solvent polarity is observed. Both these effects counterbalance and consequently τ_{fl} varies only weakly from one solvent to another.

The TCSPC measurements with CNPeDMA were complicated, especially in polar solvents, by the presence of a strongly fluorescent impurity. Although the number of solvents investigated is small, the trends found with PeDMA seem to be present with CNPeDMA as well (Table 2). However, the decrease of τ_{nr} with increasing solvent polarity is more pronounced than with PeDMA.

Fluorescence up-conversion measurements were performed with PeDMA in CHX, THF, and ACN only. In all three solvents, the intensity time profiles were found to be wavelength dependent (Figure 2). In CHX, the intensity at 450 nm, that is, at the very blue edge of the fluorescence band (Figure 1), exhibits an initial fast decay component, whereas a small rising component is present around the center of the emission band in the 480−550 nm region. These time profiles have been analyzed globally by using the sum of two exponential functions, one of them with a fixed time constant of 3.4 ns measured by TCSPC. A good fit was obtained with a time constant of 2.5 ps for the fast dynamic feature (Figure 2 top). Such early fluorescence dynamics is similar to that reported for Pe in the same solvent and assigned to vibrational cooling.[45] This process leads to a narrowing of the emission band and shows up as decaying and rising components at wavelengths coinciding with the edges and the central part of the band, respectively.

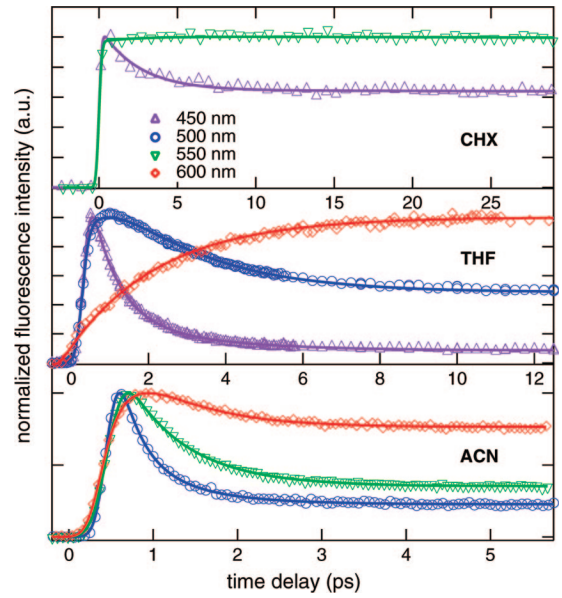

Figure 2. Wavelength and solvent dependence of the early fluorescence dynamics of PeDMA and best global multiexponential fits (solid lines).

TABLE 3: Parameters Obtained from Time-Resolved Fluorescence Measurements with PeDMA

solvent	τ_{fl1}[a] (ps)	τ_{fl2}[a] (ps)	τ_r[b] (ps)	r_0[c]
CHX	2.5		100	0.37
THF	0.66	2.4	73	0.38
PnOH[d]	160		462	0.38
ACN	0.25	0.74	51	0.36

[a] Global time constants. [b] Fluorescence anisotropy decay time. [c] Initial anisotropy. [d] Measured by TCSPC only.

In THF, the fluorescence dynamics is strongly wavelength dependent during the first 10 ps (Figure 2 middle). Afterward, the fluorescence intensity at all wavelengths decays to zero on the nanosecond time scale as found by TCSPC. The time profiles could be satisfactorily analyzed globally by using the sum of three exponential functions, one of them with the fixed time constant of 4.6 ns obtained from TCSPC and the other two, τ_{fl1} and τ_{fl2}, being listed in Table 3. The smaller of these two time constants appears as a decay at 450 nm, the far blue edge of the emission band, and as a rising component at 500 nm and longer wavelengths. On the other hand, τ_{fl2} is associated with a decay up to about 550 nm and to a rise at longer wavelengths.

The wavelength dependence of the early fluorescence dynamics in ACN is qualitatively similar to that in THF but takes place on a shorter time scale (Figure 2 bottom). The time profiles

TABLE 4: Parameters Obtained from the TA Measurements with PeDMA

solvent	τ_{TA1}[a] (ps)	τ_{TA2}[a] (ps)	$\langle\tau_{CS}\rangle$[b] (ps)	τ_{s1}[c] (ps)	τ_{s2}[c] (ps)	τ_{s3}[c] (ps)	λ_{CSS}[d] (nm)
THF	1.1	4.1	3.6	0.23	1.52		664
PnOH	18.4	114	97.4	0.67	21.7	151	683
BuOH	16	91	72	0.24	5.0	43, 133	666
BCN	4	13.4	11.2	0.36	5.3	25	671
ACN	0.55	1.65	0.67	0.09	0.63		642
DMSO	0.96	4.7	2.18	0.21	2.29	10.7	630
IL	15.7	197	141				640

[a] Global time constants. [b] Average CS time constant. [c] Solvation time constants (taken from ref 47; only time constants associated with a relative amplitude ≥0.05 are listed). [d] Absorption maximum of the CSS.

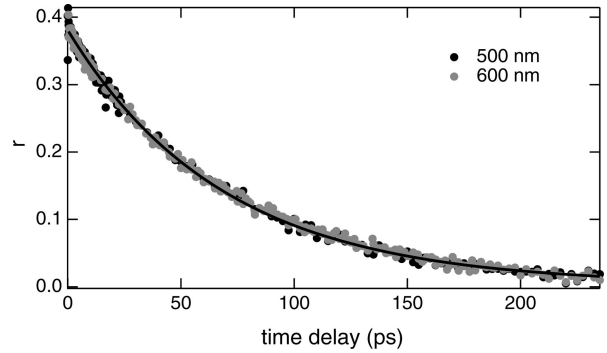

Figure 3. Decay of the fluorescence polarization anisotropy of PeDMA in THF recorded at 500 and 600 nm and best single-exponential fit (solid line).

could also be analyzed globally with the same function as in THF but with smaller time constants (Table 3). The amplitude associated with the shorter time constant is positive at 500 nm, thus corresponding to a decay, close to zero at 550 nm and negative at 600 nm, hence related to a rise. On the other hand, the larger time constant is associated with a decay at all three wavelengths. Measurements at wavelengths corresponding to the red side of the emission band were not performed.

Finally, this wavelength-dependent dynamics is much slower in PnOH and can be detected, at least partially, by TCSPC. In this case, the sum of two exponential functions with 160 ps and 4.6 ns time constants was enough to reproduce the observed time profiles. The 160 ps time constant appears as a decay below about 550 nm and as a rise at longer wavelengths.

The wavelength dependence of the early fluorescence dynamics observed in polar solvents can in principle be interpreted in two ways: (1) as a dynamic Stokes shift of the emission spectrum from a polar excited state or (2) as a transition between two excited states, the initially populated state emitting at short wavelengths and the final state fluorescing at long wavelengths. The dynamics of most solvents occurs on various time scales and is thus characterized by several time constants, with the smallest stemming from inertial motion and the largest associated with diffusive motion.[46,47] The time constants obtained from the global fit (Table 3) agree relatively well with those reported for the solvation of coumarin 153 (Table 4).[47] The departure from these values could be explained by the fact that the time constants found here have not been obtained by a proper analysis of the temporal shift of the fluorescence band maximum as should be done for a rigorous determination of the solvation dynamics.[47] Moreover, vibrational cooling as observed in CHX should also occur in the polar solvents and should thus contribute to the early dynamics, additionally to solvation. This similarity between the measured time constants and the solvation time constants supports the first hypothesis but does not agree with the solvatochromism results that point to the initial population of a LES followed by a transition to a CSS, in agreement with the second hypothesis. However, all the results can be reconciled in a hybrid model where excitation first leads to the population of a weakly polar LES with a fluorescence spectrum similar to that measured in nonpolar solvents, followed by a conversion to a CSS in polar solvents only. Indeed, the change of the fluorescence spectrum observed when going from nonpolar to polar solvents indicates that CS is only operative in the latter. Therefore, the LES-to-CSS conversion should be, at least partially, solvent controlled. As a consequence, the CSS population generated at early time is small and poorly solvated, and its fluorescence spectrum is blue-shifted relatively to the equilibrium spectrum. The population of the CSS grows with time, and its fluorescence spectrum corresponds more and more to that of the fully solvated CSS. In such a scheme, dynamics Stokes shift and CS dynamics are closely entangled, and thus, a simple precursor−successor kinetics between two populations with well-defined spectra is not observed in the fluorescence time profiles.

Time-resolved fluorescence polarization anisotropy measurements have been performed in an attempt to disentangle these two dynamics. A transition between two emitting states should be accompanied by a change of the polarization anisotropy if the associated transition dipole moments are not parallel and if this process is faster than molecular reorientation. Figure 3 shows the decay of the polarization anisotropy measured with PeDMA in THF at 500 and 600 nm. Although the time profiles of the fluorescence recorded at magic angle differ considerably at these two wavelengths (Figure 2), the anisotropy decays, $r(t)$, are the same and can be reproduced by using an exponential function with a 73 ps time constant, τ_r, and an initial anisotropy, r_0, of 0.38. Exponential decay of the polarization anisotropy was also observed in the other solvents, the best-fit parameters being listed in Table 3. A plot of τ_r versus solvent viscosity is linear with a slope of 109 ps·cP^{-1}. The latter together with the magnitude of τ_r indicate that the depolarisation of the fluorescence stems entirely from the reorientational motion of PeDMA[48,49] and is not associated with the LES to CSS transition. The r_0 value is independent of the fluorescence wavelength and ranges between 0.36 and 0.38, close to the maximum value of 0.4 for molecules where the transition dipole moments responsible for absorption and emission are parallel.[50] In the present case, excitation is performed at 400 nm and results in the population of a vibrational excited state. As already discussed for Pe, vibronic coupling with a higher electronic excited state can explain the small departure from 0.4 found here.[45] The absence of fluorescence depolarisation arising from the LES to CSS conversion suggests that the dipole moments related to LES-S_0 and CSS-S_0 transitions are parallel. This is absolutely reasonable when considering that the LES-S_0 transition dipole is oriented along the long molecular axis of Pe whereas the CSS-S_0 transition dipole should point from the DMA to the Pe units.

Transient Absorption. TA spectra recorded with PeDMA in various solvents at different time delays after 400 nm excitation are depicted in Figures 4−6. In nonpolar solvents like CHX, the shape of the TA spectra is essentially independent of time (Figure 4). The spectra consist of a negative band below 615 nm and a positive band above this wavelength. The negative band can be assigned to both stimulated emission and bleach of the S_0-LES absorption. However, the blue side of this band

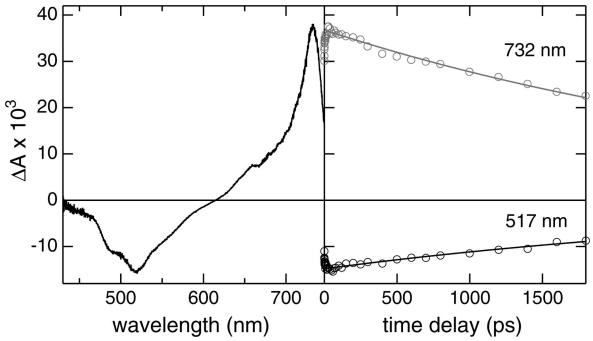

Figure 4. TA spectrum recorded 1 ps after 400 nm excitation of PeDMA in CHX (left) and temporal evolution of the TA signal intensity at different wavelengths with the best global fit (right).

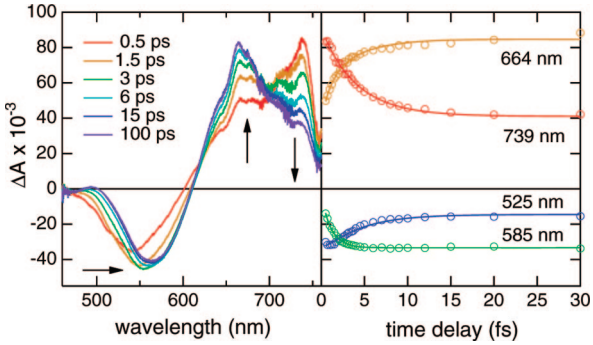

Figure 5. TA spectra recorded at various time delays after 400 nm excitation of PeDMA in THF (left) and temporal evolution of the TA signal intensity at different wavelengths with the best global fit (right).

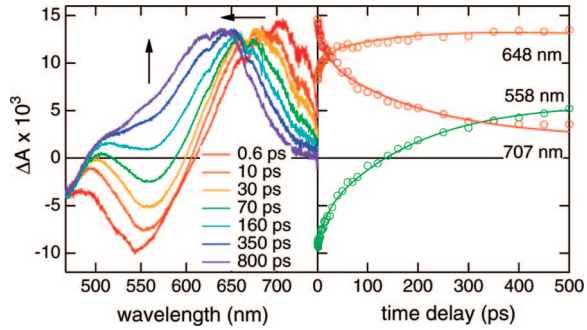

Figure 6. TA spectra recorded at various time delays after 400 nm excitation of PeDMA in IL (left) and temporal evolution of the TA signal intensity at different wavelengths with the best global fit (right).

differs from the S_0-LES absorption bleach and stimulated emission spectra pointing to the presence of an overlapping excited-state absorption. On the other hand, the positive band at 730 nm can be ascribed to LES absorption. Compared to the S_1-state absorption band of Pe, it is red-shifted by about 30 nm (590 cm^{-1}). The TA intensity shows a small initial dynamic feature with a 2−3 ps time constant that compares well with that of 2.5 ps observed by fluorescence up-conversion and ascribed to vibrational cooling. After that, the signal intensity decays slowly, in agreement with the 3.4 ns fluorescence lifetime measured by TCSPC.

A substantial temporal evolution of the TA spectrum can be observed already in medium polarity solvents as illustrated in Figure 5 with THF. The early spectrum is very similar to that observed in CHX. As time evolves, the intensity of the 730 nm band decreases and a new positive band centered at 664 nm grows. Meanwhile, the maximum of the negative band shifts to longer wavelengths. The time evolution of the TA intensity in different spectral regions can be analyzed globally by using the sum of three exponential functions, with the time constants τ_{TA1} and τ_{TA2} listed in Table 4 (Figure 5 right) additionally to that measured by TCSPC (Table 1). The small time constants match quite well those found by fluorescence up-conversion. After about 15−20 ps, the shape of the TA spectrum remains constant, and the intensity decays on the nanosecond time scale.

This spectral dynamics can be accounted for by the transition from the LES of PeDMA, which is responsible for the 730 nm TA band observed in CHX as well, to a CSS absorbing at shorter wavelengths. Contrary to the emission, the CSS absorption band does not manifest a very significant spectral shift that could be associated with solvent relaxation, indicating that the potential curves along the solvation coordinate of the initial and final states responsible for this absorption band are essentially parallel. By contrast to what was reported for ADMA, the absorption spectrum of the CSS differs substantially from those of the radical ions of the donor and acceptor moieties. Indeed, the CSS band culminates at 664 nm, whereas Pe radical anion absorbs at 580 nm and DMA cation has a weak absorption band around 475 nm.[24] This demonstrates that the degree of charge separation in this state is not unity. A similar effect has recently been reported with nitroperylene, where the absorption spectrum of the excited state was red-shifted by about 20−30 nm compared to the absorption band of Pe radical cation, denoting a partial CT.[51] This observation is also consistent with the smaller excited-state dipole moment found for PeDMA compared to that reported for ADMA.[17]

The time constants τ_{TA1} and τ_{TA2} obtained from the global analysis of the TA time profiles at different spectral regions reflect the transition from LES to CSS as well as the solvation of the CSS, as shown by the dynamic Stokes shift of the stimulated emission. Because of the latter process, a global fit over the whole spectrum with target analysis cannot be easily performed. Thus, in order to determine the relative amplitudes of τ_{TA1} and τ_{TA2} in the CS dynamics, the time profile of the TA around 664 nm, where CSS absorption dominates, was subtracted from that at 730 nm, after normalization of the intensities at long time delays, where TA at both wavelengths is due to the CSS population only. The resulting time profile reflects the temporal evolution of LES population only. Analysis of the later shows that the relative amplitudes of the 1.1 and 4.1 ps components in the CS dynamics amount to 0.16 and 0.84, respectively, giving an average time constant $\langle\tau_{CS}\rangle$ of 3.6 ps.

In more polar solvents, such as ACN, DMSO, and IL, biphasic spectral dynamics qualitatively similar to that in THF is observed (Figure 6). The time constants obtained from global analysis are on the same order of magnitude as those reported for solvation (Table 4).[47] The early TA spectrum is dominated by the LES band, which culminates at 730 nm, whereas the late spectrum arising from the CSS population peaks at a wavelength that is solvent dependent. The average time constant for the LES-to-CSS transition, determined as described above, as well as the peak wavelength of the CSS absorption band are listed in Table 4. This table and Figure 7 illustrate the solvent dependence of the CSS band maximum and its shift toward shorter wavelengths with increasing polarity. Note that in TOL, both LES and CSS are probably in equilibrium (see below). As anticipated earlier from the radiative time constants τ_{rad}, this suggests that the nature of this state and its degree of charge separation depend on the solvent polarity. In principle, such an effect should appear as a deviation from the linear dependence of the steady-state emission maximum on the polarity function.[19]

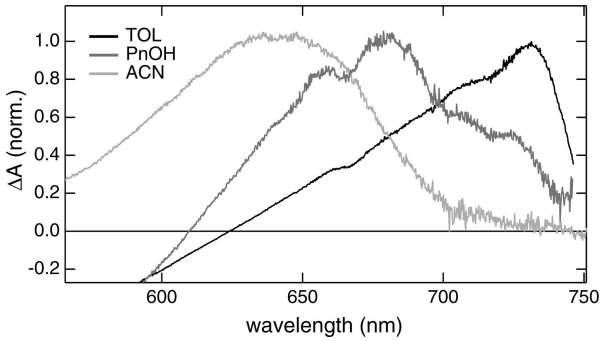

Figure 7. Solvent dependence of the TA spectrum recorded with PeDMA at long time delay.

As shown in Figure S3 (see Supporting Information), some nonlinearity in the solvatochromic plot of PeDMA emission cannot be excluded.

The CS dynamics in IL is extremely multiphasic and involves a large range of time scales. This agrees well with the solvation dynamics of similar ionic liquids that has been reported to present few picoseconds to subnanosecond components.[52,53] Apart from the time scale, the shape of the TA spectra are very similar to those measured in DMSO, indicating that these two solvents have a similar effective polarity. This is further supported by the position of the stationary absorption and fluorescence maxima (Table 1).

Finally, the TA spectra recorded with PeDMA in the weakly polar TOL are intermediates between those measured in CHX and in THF (Figure S5, see Supporting Information). The early spectra are very similar to those found in CHX, and as time proceeds, a shoulder at 700 nm, that is, at the blue side of the LES absorption band, grows, whereas the negative TA band shifts to the red. At time delays longer than about 20 ps, the TA spectral shape remains unchanged, and the maximum at 730 nm is still clearly visible. Both CSS and LES most probably contribute to the late TA spectrum, pointing to an equilibrium between these two states. The coexistence of both excited-state populations cannot really be inferred from stationary fluorescence because both LES and CSS emission spectra are probably strongly overlapping.

The time constants obtained from TA and those found by time-resolved fluorescence are not identical but are still very close and similar to the time constants of solvation (Tables 3 and 4). Actually, they reflect essentially the same phenomenon, namely, a solvent-controlled transition between two excited states. However, this process manifests differently in time-resolved fluorescence and TA. Indeed, the early fluorescence dynamics is dominated by a large and continuous change of the emission spectrum, as the spectra of the initial and final states cannot be really distinguished. On the other hand, a rather clear precursor−successor kinetics can be seen in the early TA spectra above 600−650 nm. As a consequence, the time constants obtained from global analysis of the fluorescence data could differ from those resulting from a global analysis of the TA data. However, because of the presence of a precursor−successor kinetics, the TA time constants are probably a better estimate of the CS dynamics.

Additionally to the solvent coordinate, the twist angle between the DMA and anthracene groups was proposed to play an important role in the CS dynamics of ADMA.[20] Our data do not allow any conclusion to be drawn on the involvement of this coordinate in the case of PeDMA.

A strong solvent dependence can also be observed in the TA spectra recorded with CNPeDMA upon 490 nm excitation

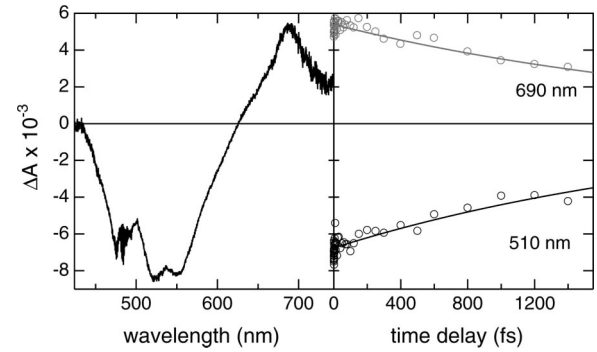

Figure 8. TA spectra recorded 1 ps after 490 nm excitation of CNPeDMA in CHX (left, the noise around 490 nm is due to imperfect elimination of the scattered pump light) and temporal evolution of the TA signal intensity at different wavelengths with the best global fit (right).

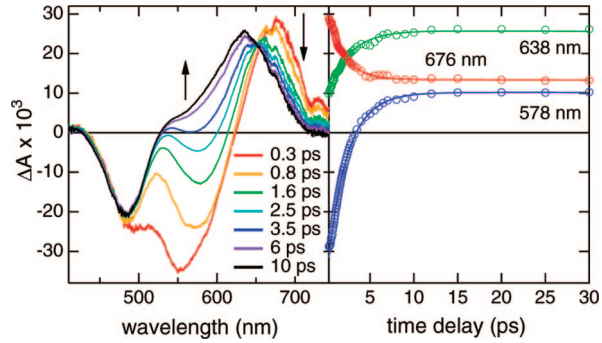

Figure 9. TA spectra recorded at various time delays after 490 nm excitation of CNPeDMA in THF (left) and temporal evolution of the TA signal intensity at different wavelengths with the best global fit (right).

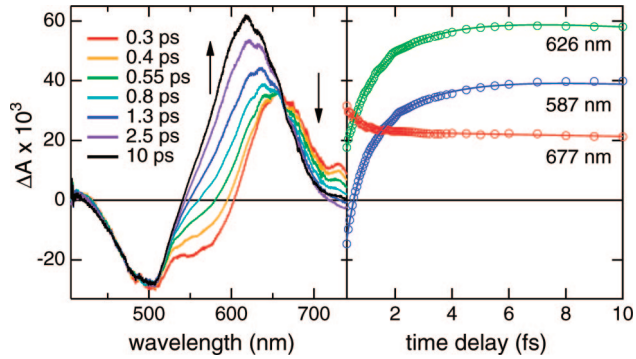

Figure 10. TA spectra recorded at various time delays after 490 nm excitation of CNPeDMA in DMSO (left) and temporal evolution of the TA signal intensity at different wavelengths with the best global fit (right).

(Figures 8−10). No significant spectral dynamics can be observed in CHX. The TA spectra consist of a positive band peaking at 690 nm that can be ascribed to the LES absorption and a negative band between 400 and 650 nm arising from both stimulated emission and bleaching of the S_0-LES absorption (Figure 8). The blue shift of the LES absorption band found with CNPeDMA relatively to PeDMA can also be found in the S_1-state absorption of CNPe relatively to Pe.[26] Contrary to PeDMA in CHX, no initial dynamic feature that could be ascribed to vibrational cooling is observed with CNPeDMA. This is consistent with the smaller excess excitation energy deposited in CNPeDMA at 490 nm (0.13 eV) compared to PeDMA at 400 nm (0.44 eV). Consequently, after a prompt

TABLE 5: Parameters Obtained from the TA Measurements with CNPeDMA

solvent	τ_{TA1}[a] (ps)	τ_{TA2}[a] (ps)	$\langle\tau_{CS}\rangle$[b] (ps)
THF	1.8	2.6	1.8
ACN	0.18	0.63	0.18
DMSO	0.48	1.9	0.48

[a] Global time constants. [b] Average CS time constant.

rise, the TA intensity decays on the nanosecond time scale, in agreement with the 3.6 ns fluorescence lifetime.

Strong spectral dynamics is observed in the other solvents investigated, namely, THF, ACN, and DMSO. In the less polar THF (Figure 9), the early TA spectrum is quite similar to that in CHX apart from the shape of the stimulated emission band. At later times, the LES absorption band decreases; the stimulated emission band shifts to the red and is gradually replaced by a positive TA band centered at 634 nm. Meanwhile, the negative TA band due to the bleach of the S_0-LES absorption remains unchanged. As shown in Figure 9, the time evolution of the TA intensity at various wavelengths throughout the spectral window can also be analyzed globally with the sum of three exponential functions, with two time constants associated with the early dynamics, τ_{TA1} and τ_{TA2} (Table 5) and the time constant measured by TCSPC. The LES population dynamics was determined as described above for PeDMA in THF, and the average CS time constant are listed in Table 5.

In more polar solvents, the spectral dynamics is qualitatively similar, the main difference being a weaker stimulated emission (Figure 10). In this case again, a global analysis with three exponential functions can correctly reproduce the time profile of the TA intensity at various wavelengths, the resulting time constants, and the average CS time constant being listed in Table 5.

Comparison of the CS Dynamics in PeDMA and CNPeDMA. The above results show that the excited-state dynamics of PeDMA and CNPeDMA do not differ very strongly. In both cases, optical excitation leads to the population of an excited state characterized by a charge distribution rather similar to that of the ground state, a LES. Because of this, a very small solvatochromism of the first electronic absorption band is observed. In nonpolar solvents, the LES population decays entirely radiatively as evidenced by a fluorescence quantum yield of unity.

In polar solvents, the LES population converts rapidly to the CSS, which presents a large electric dipole moment as testified by the important solvatochromism of its fluorescence. The two time constants associated with the early TA dynamics measured with PeDMA and CNPeDMA are relatively close to those reported for solvation dynamics (Table 4), with the probable origins of the differences discussed above.

Table 4 shows that the average CS time constant for PeDMA is in most solvents close to the larger solvation time constant. For CNPeDMA on the other hand, CS in polar solvents takes place on a time scale similar to that of the fastest solvation component, associated with inertial solvent motion. This indicates that partial solvation is enough to enable full conversion of the LES population of CNPeDMA. The solvation energy gained within the time scale of inertial motion of the solvent molecules gives a sufficient driving force to enable ultrafast CS. In the less polar THF, additional solvation energy occurring within the time scale of diffusive solvent motion is required, and in this case, the CS time constant is close to the diffusive solvation time as also found with PeDMA.

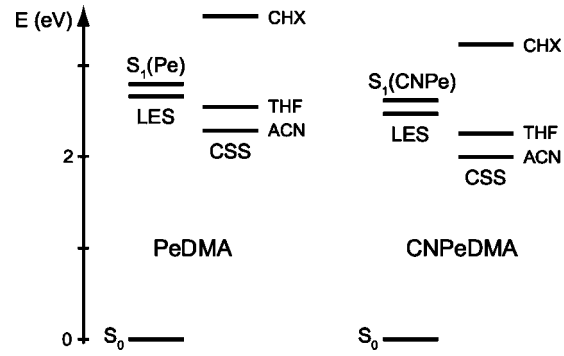

Figure 11. Energy level scheme pertaining to the CS dynamics in PeDMA and CNPeDMA in different solvents (the energies of the CSS have been calculated by assuming full charge separation).

The difference between PeDMA and CNPeDMA arises most probably from a more favorable driving force in CNPeDMA as illustrated in Figure 11. By using the reduction potentials and the S_1-energies reported in ref 25 for Pe and CNPe, the free energy for full CS, ΔG_{CS}, in PeDMA and CNPeDMA calculated from the Weller equation[54] can be estimated to -0.2 and -0.3 eV in THF and -0.5 and -0.6 eV in ACN, respectively. In CHX, ΔG_{CS} is largely positive for both compounds, in agreement with the absence of CS. If the energy of the LES is used instead of the S_1-energy of the chromophoric unit, the result is qualitatively the same except that the driving force for CS is smaller by about 0.15 eV (Figure 11). Therefore, because of a larger driving force, CS in CNPeDMA requires less solvation compared to CS in PeDMA to be ultrafast.

Comparison with Pe and CNPe in Pure DMA. The fluorescence quenching of Pe and CNPe in pure DMA has been reported to take place with average time constants of 4.9 ps and 420 fs, respectively.[25] This difference is much larger than that found here between PeDMA and CNPeDMA in THF, which has a dielectric constant similar to that of DMA, as well as in ACN and DMSO. A more favorable driving force can account for the relatively small difference found here between PeDMA and CNPeDMA but not for those measured in pure DMA. Therefore, the results obtained here strongly support the model used to account for the large differences found in DMA and invoking a larger number of donor molecules with an optimal orientation for CS with CNPe.

Interestingly, the intrinsic intermolecular CS time constant of $\sim$1 ps deduced from this orientational model is on the same order of magnitude as the intramolecular τ_{CS} found here in THF. This indicates that the electronic coupling for this process, V_{CS}, has a similar magnitude in both cases or, alternatively, that V_{CS} is so large that both intra- and intermolecular CS are fully solvent controlled. The latter possibility agrees with the results obtained here as well as with the time constant of 1.1 ps observed in the solvation dynamics of DMA.[55]

The quenching product of Pe and CNPe in pure DMA was shown to be an exciplex exhibiting fluorescence with a maximum at 570 and 650 nm, respectively. These peak wavelengths compare well with those found here with PeDMA and CNPeDMA in THF. Because an exciplex is a bimolecular complex with some extent of charge separation,[56] it is similar to an intermolecular CSS. Thus, both denominations will be used here without distinction. The parameters associated with the exciplex emission of Pe and CNPe in DMA and with the emission of the DA compounds in THF are compared in Table 6. It appears that the decay times and especially the quantum yields of inter- and intramolecular emission are very dissimilar.

TABLE 6: Photophysical Parameters Related to Linked and Non-Linked DA Systems

	$\langle\tau_{CS}\rangle^a$ (ps)	λ_{fl}^b (nm)	Φ_{fl}^c	τ_{fl}^d (ns)	$\tau_{rad}n^{3\,e}$ (ns)	τ_{nr}^f (ns)
Pe in DMA[g]	1.2	570	0.04	37.0	3490	38.5
PeDMA in THF	1.8	556	0.77	4.6	16.5	20.0
CNPe in DMA[g]	1.2	650	$1.1\cdot10^{-4}$	1.6	5480	1.6
CNPeDMA in THF	3.6	622	0.59	4.5	21.1	11.0

[a] Average CS time constant. [b] Fluorescence maximum. [c] Fluorescence quantum yield. [d] Fluorescence lifetime. [e] Solvent-corrected radiative time constant. [f] Nonradiative time constant. [g] Taken from ref 26.

This difference stems essentially from the radiative time constant, τ_{rad}, that is much smaller in the intramolecular cases. However, the nonradiative time constants are of the same order of magnitude for both intra- and intermolecular cases. This nonradiative deactivation is essentially a CR process the dynamics of which depends on several parameters such as the driving force, ΔG_{CR}, the reorganization energy, λ, and the electronic coupling constant V_{CR}.[57] Because no very big difference in ΔG_{CR} and λ is expected between intra- and intermolecular CR, the likeness of the τ_{nr} values shown in Table 6 points to a rather similar magnitude of V_{CR} as well.

The substantially slower nonradiative deactivation observed with PeDMA compared to CNPeDMA can be accounted for by a difference in ΔG_{CR} (Figure 11). The latter, calculated by assuming full CS in ACN, amounts to −2.3 and −2.0 eV for PeDMA and CNPeDMA, respectively. Therefore, CR in PeDMA is more in the inverted regime than in CNPeDMA and is thus slower,[57] as already discussed in detail for Pe and CNPe in pure DMA.[26] This result can be equivalently explained by a larger energy gap for nonradiative deactivation with PeDMA relative to CNPeDMA.[58]

The large difference in τ_{rad} can be clarified by considering that this quantity is proportional to $|\vec{\mu}_{CT}|^{-2}$, where $\vec{\mu}_{CT}$ is the transition dipole moment associated with the observed CT fluorescence. It has been shown that the wave function of the CSS can be described as a linear combination of the pure ion-pair state, IPS, and LES wave functions. As a consequence, τ_{rad} depends on the fractional ion pair character of the CSS, f_{IPS}, and on the angle θ between $\vec{\mu}_{IPS}$ and $\vec{\mu}_{LES}$, the transition dipole moments for the emission from the IPS and from the LES, respectively:[59,60]

$$\tau_{rad}^{-1} \propto |\vec{\mu}_{CT}|^2 = f_{IPS}|\vec{\mu}_{IPS}|^2 + f_{LES}|\vec{\mu}_{LES}|^2 - 2f_{IPS}^{1/2}f_{LES}^{1/2}|\vec{\mu}_{IPS}||\vec{\mu}_{LES}|\cos\theta \quad (1)$$

where $f_{LES} = 1 - f_{IPS}$. f_{IPS} depends mainly on the energy difference between the IPS and the LES and can be expected to be similar for the inter- and the intramolecular CSS. This is supported by the peak positions of the emission band, which are not very distant. However, θ should be around 180° in the linked DA systems, as confirmed by the fluorescence polarization anisotropy, whereas it should be close to 90° in the bimolecular exciplexes, because it is generally accepted that their two constituents have a sandwich-like coplanar orientation. Therefore, this expression predicts a much stronger LES intensity borrowing in the CT emission of the linked DA systems and thus a small τ_{rad}, in agreement with the observation.

On the other hand, the magnitude of $\vec{\mu}_{IPS}$ is proportional to the electronic coupling between the IPS and the neutral ground state, which is also a key parameter for CR. Therefore, the decrease of τ_{rad} observed when going from intra- to intermolecular CSS cannot be accounted for by a smaller coupling constant, because in this case, intramolecular CR would be much faster than intermolecular CR, contrary to the observation (Table 6).

Concluding Remarks

This investigation shows that Pe is perfectly well suited as electron acceptor in covalently linked DA compound because it gives strong spectroscopic signatures that allow the nature of the excited state to be precisely determined. Although the excited-state dynamics of PeDMA and CNPeDMA are not largely dissimilar from that of the well-studied ADMA, a few differences should be noted. First, the absorption spectra of the CSS of PeDMA and CNPeDMA are clearly not the same as those of the pure ion pair, indicating that the extent of CS in this state is inferior to one. Second, the CS dynamics in PeDMA is solvent controlled, whereas that in ADMA was reported to be somewhat slower. Possible reasons for these differences might be the driving force, the reduction potential of anthracene in the S_1 state being 0.25 V higher than that of Pe, and/or a larger twist angle of the DMA unit resulting in a larger decoupling of the donor and acceptor units. This would also be consistent with the larger excited-state dipole moment reported for ADMA.[17]

It should also be noted that the dynamics measured here with PeDMA and CNPeDMA in ACN agrees also with that reported with PhDMA in the same solvent, where CS was found to take place on a subpicosecond time scale.

This study also reveals that the excited-state dynamics of Pe and CNPe covalently linked to DMA in medium polarity solvents share many similarities with that of Pe and CNPe in pure DMA: CS from one DMA to the acceptor occurs on a similar time scale, the resulting emission spectra are alike, and the nonradiative deactivation times are comparable. Therefore, the electronic coupling constants for CS and CR should be about the same order of magnitude independently on whether the process is intra- and intermolecular. This is rather surprising and might be purely coincidental because the mutual orientations of the D and A units can be expected to be very dissimilar. On the other hand, the structure of the CSS is responsible for the strong difference in the quantum yield of emission, because it affects the radiative time constant through the coupling between the transition dipole moment for pure ion pair state and LES emission. This comparison between inter- and intramolecular systems gives a new insight into the influence mutual orientation of the reactants on CS dynamics, on the nature of ensuing product, and on its CR dynamics.

Acknowledgment. This work was supported by the Fonds National Suisse de la Recherche Scientifique through Project no. 200020-115942.

Supporting Information Available: Synthesis of CNPeDMA, absorption spectra of PeDMA and CNPeDMA down to 250 nm, solvatochromic plots of PeDMA, fluorescence decay of PeDMA recorded by TCSPC, TA spectra of PeDMA in toluene, and calculation of the transition dipole moment. This information is available free of charge via the Internet at http://pubs.acs.org.

References and Notes

(1) Leonhart, H.; Weller, A. *Z. Phys. Chem. N. F.* **1961**, 277.

(2) Electron Transfer: from isolated molecules to biomolecules. In *Adv. Chem. Phys.*; Jortner, J., Ed.; 1999; Vol. 106−107.

(3) Adams, D. M.; Brus, L.; Chidsey, C. E. D.; Creager, S.; Creutz, C.; Kagan, C. R.; Kamat, P. V.; Lieberman, M.; Lindsay, S.; Marcus, R. A.; Metzger, R. M.; Michel-Beyerle, M. E.; Miller, J. R.; Newton, M. D.; Rolison, D. R.; Sankey, O.; Schanze, K. S.; Yardley, J.; Zhu, X. *J. Phys. Chem. B* **2003**, *107*, 6668.

(4) Grabowski, Z. R.; Rotkiewicz, K.; Rettig, W. *Chem. Rev.* **2003**, *103*, 3899.
(5) Guldi, D. M.; Rahman, G. M. A.; Zerbetto, F.; Prato, M. *Acc. Chem. Res.* **2005**, *38*, 871.
(6) Kodis, G.; Terazono, Y.; Liddell, P. A.; Andréasson, J.; Garg, V.; Hambourger, M.; Moore, T. A.; Moore, A. L.; Gust, D. *J. Am. Chem. Soc.* **2006**, *128*, 1818.
(7) Bhosale, S.; L., S. A.; Talukdar, P.; Fürstenberg, A.; Banerji, N.; Vauthey, E.; Bollot, G.; Mareda, J.; Ë; oger, C.; Würthner, F.; Sakai, N.; Matile, S. *Science* **2006**, *313*, 84.
(8) Wasielewski, M. R. *J. Org. Chem.* **2006**, *71*, 5051.
(9) Li, W.-S.; Kim, K. S.; Jiang, D.-L.; Tanaka, H.; Kawai, T.; Kwon, J. H.; Kim, D.; Aida, T. *J. Am. Chem. Soc.* **2006**, *128*, 10527.
(10) Ware, W. R.; Richter, H. P. *J. Chem. Phys.* **1968**, *48*, 1595.
(11) Mataga, N.; Asahi, T.; Kanda, Y.; Okada, T.; Kakitani, T. *Chem. Phys.* **1988**, *127*, 249.
(12) Lewitzka, F.; Löhmannsröben, H.-G. *Z. Phys. Chem.* **1990**, *169*, 203.
(13) Anner, O.; Haas, Y. *Chem. Phys. Lett.* **1985**, *119*, 199.
(14) Vauthey, E. *J. Phys. Chem. A* **2000**, *104*, 1804.
(15) Vauthey, E. *J. Phys. Chem. A* **2001**, *105*, 340.
(16) Muller, P.-A.; Vauthey, E. *J. Phys. Chem. A* **2001**, *105*, 5994.
(17) Okada, T.; Kawai, M.; Ikemachi, T.; Mataga, N.; Sakata, Y.; Misumi, S.; Shionoya, S. *J. Phys. Chem.* **1984**, *88*, 1976.
(18) Tominaga, K.; Walker, G. C.; Jarzeba, W.; Barbara, P. F. *J. Phys. Chem.* **1991**, *95*, 10475.
(19) Herbich, J.; Kapturkiewicz, A. *Chem. Phys.* **1993**, *170*, 221.
(20) Martin, M. M.; Plaza, P.; Changenet-Barret, P.; Siemiarczuk, A. *J. Phys. Chem. A* **2002**, *106*, 2351.
(21) Techert, S.; Wiessner, A.; Schmatz, S.; Staerk, H. *J. Phys. Chem. B* **2001**, *105*, 7579.
(22) Onkelinx, A.; Schweitzer, G.; De Schryver, F. C.; Miyasaka, H.; Van der Auweraer, M.; Asahi, T.; Masuhara, H.; Fukumura, H.; Yashima, A.; Iwai, K. *J. Phys. Chem. A* **1997**, *101*, 5054.
(23) Baumann, W.; Bischof, H.; Fröhling, J. C.; Brittinger, C.; Rettig, W.; Rotkiewicz, K. *J. Photochem. Photobiol.* **1992**, *A64*, 49.
(24) Shida, T. *Electronic Absorption Spectra of Radical Ions*; Elsevier: Amsterdam, 1988; Vol. Physical Sciences data 34.
(25) Morandeira, A.; Fürstenberg, A.; Gumy, J.-C.; Vauthey, E. *J. Phys. Chem. A* **2003**, *107*, 5375.
(26) Morandeira, A.; Fürstenberg, A.; Vauthey, E. *J. Phys. Chem. A* **2004**, *108*, 8190.
(27) Barabanov, I. I.; Korolev, V. V.; Gritsan, N. P.; Vauthey, E. *Mendeleev Commun.* **2006**, *16*, 226.
(28) Murov, S. L.; Carmichael, I.; Hug, G. L. *Handbook of Photochemistry*; Marcel Dekker Inc.: New York, 1993.
(29) Fürstenberg, A.; Julliard, M. D.; Deligeorgiev, T. G.; Gadjev, N. I.; Vassilev, A. A.; Vauthey, E. *J. Am. Chem. Soc.* **2006**, *128*, 7661.
(30) Morandeira, A.; Engeli, L.; Vauthey, E. *J. Phys. Chem. A* **2002**, *106*, 4833.
(31) Duvanel, G.; Banerji, N.; Vauthey, E. *J. Phys. Chem. A* **2007**, *111*, 5361.
(32) Perdew, J. P. *Phys. Rev. B* **1986**, *33*, 8822.
(33) Ahlrichs, R.; Bär, M.; Häser, M. *Chem. Phys. Lett.* **1989**, *162*, 165.
(34) Riddick, J. A.; Bunger, W. B. *Organic Solvents*; J. Wiley: New York, 1970.
(35) Onsager, L. *J. Am. Chem. Soc.* **1936**, *58*, 1486.
(36) Suppan, P. *J. Photochem. Photobiol.* **1990**, *A50*, 293.
(37) Edward, J. T. *J. Chem. Educ.* **1970**, *4*, 261.
(38) Techert, S.; Schmatz, S.; Wiessner, A.; Staerk, H. *J. Phys. Chem. A* **2000**, *104*, 5700.
(39) Baumann, W.; Schwager, B.; Detzer, N.; Okada, T.; Mataga, N. *Bull. Chem. Soc. Jpn.* **1987**, *60*, 4245.
(40) Herbich, J.; Kapturkiewicz, A. *J. Am. Chem. Soc.* **1998**, *120*, 1014.
(41) McRae, E. G. *J. Phys. Chem.* **1957**, *61*, 562.
(42) Herbich, J.; Kapturkiewicz, A. *Chem. Phys.* **1991**, *158*, 143.
(43) Strickler, S. J.; Berg, R. A. *J. Chem. Phys.* **1962**, *37*, 814.
(44) Birks, J. B. *Photophysics of Aromatic Molecules*; Wiley: New York, 1970.
(45) Pigliucci, A.; Duvanel, G.; Lawson Daku, M. L.; Vauthey, E. *J. Phys. Chem. A* **2007**, *111*, 6135.
(46) Rosenthal, S. J.; Xie, X.; Du, M.; Fleming, G. R. *J. Chem. Phys.* **1991**, *95*, 4715.
(47) Horng, M. L.; Gardecki, J. A.; Papazyan, A.; Maroncelli, M. *J. Phys. Chem.* **1995**, *99*, 17311.
(48) Vauthey, E. *Chem. Phys. Lett.* **1993**, *216*, 530.
(49) Williams, A. M.; Jiang, Y.; Ben-Amotz, D. *Chem. Phys.* **1994**, *180*, 119.
(50) Fleming, G. R. *Chemical Applications of Ultrafast Spectroscopy*; Oxford University Press: New York, 1986.
(51) Mohammed, O. F.; Vauthey, E. *J. Phys. Chem. A* **2008**, *112*, 3823.
(52) Lang, B.; Angulo, G.; Vauthey, E. *J. Phys. Chem. A* **2006**, *110*, 7028.
(53) Arzhantsev, S.; Jin, H.; Baker, G. A.; Maroncelli, M. *J. Phys. Chem. B* **2007**, *111*, 4978.
(54) Weller, A. *Z. Phys. Chem. N. F.* **1982**, *133*, 93.
(55) Xu, Q.-H.; Scholes, G. D.; Yang, M.; Fleming, G. R. *J. Phys. Chem. A* **1999**, 10348.
(56) Braslavsky, S. E. *Pure Appl. Chem.* **2007**, *79*, 293.
(57) Marcus, R. A.; Sutin, N. *Biochim. Biophys. Acta* **1985**, *811*, 265.
(58) Siebrand, W. *J. Chem. Phys.* **1971**, 55.
(59) Gould, I. R.; Young, R. H.; Mueller, L. J.; Albrecht, A. C.; Farid, S. *J. Am. Chem. Soc.* **1994**, *116*, 8188.
(60) Arnold, B. R.; Euler, A.; Poliakov, P. V.; Schill, A. W. *J. Phys. Chem. A* **2001**, *105*, 10404.

JP803621Z